Assessing the vulnerability of a Dutch river dyke to rising water levels

Cormac Reale
Lecturer, Dept. of Architecture and Civil Engineering, University of Bath, Bath, United Kingdom

Aryan Gupta
Research Engineer, InGeo, Delft, Netherlands

Tom De Gast
Senior Engineer, Waterschap Hollandse Delta, Ridderkerk, Netherlands & Researcher, Dept. of Geoscience & Engineering, Delft University of Technology, Delft, Netherlands

Kenneth Gavin
Professor, Dept. of Geoscience & Engineering, Delft University of Technology, Delft, Netherlands

ABSTRACT: Dykes provide protection from the risk of flooding to approximately 60% of the Netherlands, by area. Unfortunately, most of the country's major cities lie within this zone, placing a large proportion of the population at risk should these flood defences fail. In total the Netherlands have over 3800 km of primary flood defences protecting the coast and inland river systems with another 14000km protecting individual polders. Recent flood events in Europe caused by extreme rainfall have raised concerns about the ability of the Dutch river dykes to resist similar events. This paper describes a quantitative assessment of the vulnerability to flooding of a primary river dyke outside Dordrecht. The dyke has shown significant signs of distress over recent years developing large tension cracks during periods of drought on its leeward side, which have progressively increased in size. It is regularly inspected by the local water authority due to its concerning visible deterioration. In this study, soil uncertainty is quantified from in-situ geotechnical tests and laboratory tests. Several failure mechanisms are then considered probabilistically, namely global stability, rapid drawdown, internal erosion and overtopping. Fragility curves are generated for each failure mechanism describing how the probability of failure would change if a given flood level were to occur, event trees are used to link the individual failure mechanisms and quantify the system probability of failure. This paper illustrates the use of fragility curves for earthwork asset management and advantages and limitations of the methodology utilised are discussed.

1. INTRODUCTION

Flood defences are critically important for the protection of people and infrastructure in low-lying areas. In the Netherlands approximately 60% of the country, by area, is below sea-level and at risk of flooding. The majority of the Dutch population and consequently most of the major cities are found in this region. To prevent flood inundation the Netherlands has constructed over 17,800 km of flood defences, 3,800 km of which are considering primary dykes as they protect the coast and inland river systems, with the remainder surrounding inland polder systems. Given the high consequences of failure maintaining and managing these flood defences is of utmost importance in The Netherlands (Rijkswaterstaat, 2014). Currently, the Dutch government spends approximately 1 billion euros a year maintaining and updating this infrastructure (Hicks *et al.*, 2019).

The Dutch substructure is characterised by easily compressible peat and clay soil layers, which can lead to large surface settlements and embankment degradation over time. This combined

with recent extreme rainfall events have raised concerns about the stability of certain Dutch river dykes under adverse conditions.

This paper describes a quantitative assessment of the vulnerability to flooding of a primary river dyke, Oostmolendijk, located just outside Dordrecht. Global stability, rapid drawdown, overtopping and internal erosion failure mechanisms were considered using a combination of in-situ geotechnical investigations and laboratory testing. A series of fragility curves were produced describing the embankments vulnerability to rising water levels.

2. SITE HISTORY AND CONDITIONS

The case study area "Oostmolendijk" is located between the towns of Ridderkerk and Hendrik-Ido-Ambacht, along the river Noord in the Zuid-Holland province of the Netherlands. Oostmolendijk is a small part of the greater dyke ring IJssel-monde also known as dijkring 17. Whilst most of the dyke ring is considered stable, Oostmolendijk considered here is affected by continuous ground settlement and cracking of the road surface resulting in ongoing maintenance problems.

Archive data shows that prior remedial work was attempted at Oostmolendijk between 1962 and 1968, however pore pressure variation during the work led to regular cracking and settlement issues caused significant delays in construction. In 2013, during further repair works a section of the dyke suffered a global shear failure. This was due to the construction of a berm, which was meant to reinforce the dyke, overloading underlying soft peat and clay layers.

The predicted flood levels associated with key return periods for Oostmolendijk are shown in Table 1. This data is sourced from Hydra-NL a probabilistic model provided by the Dutch government which calculates the statistics of hydraulic loads specifically for the assessment of primary dykes in the Netherlands.

2.1. Dyke Geometry and Soil Stratigraphy

The dyke has a height of approximately +4.7m NAP (Amsterdam Datum Level) with a small berm providing support at approximately +2m NAP. The dyke is adjacent to a small drainage ditch on the field side, see Figure 1. The field side has suffered large, localised movements with several deep tension cracks running along its face.

Table 1 Flood levels associated with key return periods at Oostmolendijk

Return Period **(years)**	Flood Level **(m+NAP)**
10	2.750
30	2.918
100	3.087
300	3.215
1000	3.342
3000	3.432
10000	3.543
30000	3.658
100000	3.826

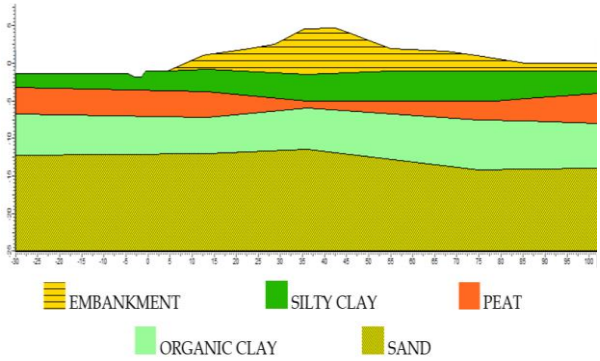

Figure 1 Geometry and interpreted soil stratigraphy

Cone penetration tests (CPT) were carried out along the embankment at regular intervals, both on the dyke and in the field adjacent, see Figure 2. The CPTs show a relatively uniform profile consisting of Holocene era soft soil deposits to a depth of 12 m below NAP overlying Pleistocene era coarse sands to great depth, see Figure 2. Investigation boreholes at the site indicate that there are three different soft soil layers present within the Holocene deposits. An upper organic silty clay layer overlying a peat layer, which is in turn underlain by a lower clay. The exact depths and thicknesses of these layers vary across the site with the peat layer in particular showing

significant compression underneath the embankment.

The dyke core is made of a medium to fine sand, with a small percentage of silt and is capped with a clay cover to prevent water ingress and egress.

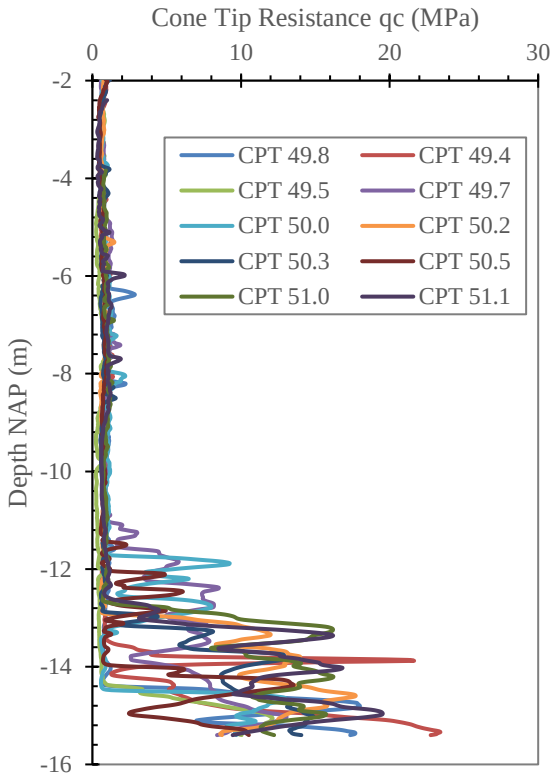

Figure 2 CPT traces at Oostmolendijk showing soft clay and peat layers extending to approximately 12m NAP

Laboratory tests were carried out to determine the strength, stiffness, and deformation characteristics of the material. It should be noted that no laboratory testing was carried out on the dyke material itself. In the clay layers, the consolidated anisotropically undrained (CAU) triaxial test was used to determine undrained shear strength, while the direct simple shear (DSS) was used in the peat layer as per standard Dutch practice. The results of these tests was used to develop a site-specific transformation factor (N_{kt}) to relate laboratory undrained strength tests at discrete locations to continuous CPT tip resistance profiles. This was achieved using the following formulae

$$s_u = \frac{q_t - \sigma_{v0}}{N_{kt}} \quad (1)$$

where

$$q_t = q_c + (1 - \alpha)u_2 \quad (2)$$

where N_{kt} is an empirical correlation factor, σ_{v0} is the total vertical stress, q_t is the corrected tip resistance, q_c is the measured CPT tip resistance , u_2 is the pore pressure measured at the cone shoulder position and α is a cone factor (typically equal to 0.15). The laboratory measured undrained shear strength values (s_u) plotted at their respective depths are compared with the cone derived s_u values for an N_{kt} of 15 in Figure 3.

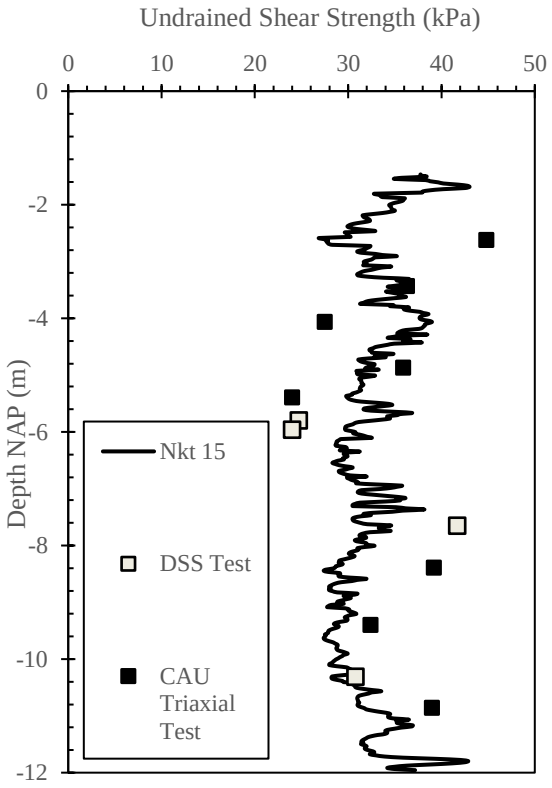

Figure 3 Undrained shear strength in the soft soil layers derived from CPT correlations compared to laboratory measurements for an N_{kt} of 15

The mean s_u values for the soft soil layers and their respective coefficients of variation were derived using the transformation described in Eq. 1, considering all the CPT traces at the site. Variation coefficients for the fill layer and the lower

Pleistocene sand were taken from a Fugro geotechnical investigation report on the dyke. The geotechnical parameters used in the analysis are shown in Table 2.

Table 2 Geotechnical parameters

Material	γ_s (kN/m^3)	s_u (kPa)	ϕ (°)	COV
Fill	20	$s_{u,top}$: 44 $s_{u,bottom}$: 41	0	0.30*
Silty Clay	16	$s_{u,top}$: 35 $s_{u,bottom}$: 30	0	0.32
Peat	11	$s_{u,top}$: 32 $s_{u,bottom}$: 29	0	0.28
Clay	18	$s_{u,top}$: 30 $s_{u,bottom}$: 33	0	0.25
Sand	20	-	35	0.23*

*Variation coefficients as given in Geotechnical Investigation report (Fugro 2020).

3. METHODOLOGY

3.1. Failure states

Dykes can fail through a wide variety of different failure mechanisms, four failure mechanisms were considered in this study global instability, internal erosion, dyke overtopping and rapid drawdown following flooding. The Morgenstern and Price (1965) general limit equilibrium method was used in SLOPE W to analyse global instability, and rapid drawdown where the water level on the river side of the slope experiences a rapid reduction in level, after a flood event. The performance function for global instability and rapid drawdown is given in Eq. 3 where FOS is the factor of safety of the slope defined as its capacity divided by its demand.

$$G(X) = FOS - 1 \quad (3)$$

Internal erosion is when particles within the dyke are eroded due to internal seepage, leading to a continuous erosion channel allowing water to flow freely from one side of the dyke to another. At which point the dyke is breached The speed at which this occurs is a function of the permeability of the material and the pore pressure head. Internal erosion has been modelled using Sellmeijers (1988) equations in this study, the model calculates the critical head difference $\Delta H_c\,[m]$, which is the largest head difference that can be sustained before internal erosion occurs. If the change in pressure head ΔH is greater than ΔH_c then failure occurs, see Eq. 4.

$$G(X) = \Delta H_c - \Delta H \quad (4)$$

Overtopping failures occur when water flows over the top of an embankment or levee. For this to occur the flood level has to be in excess of the height of the dyke making this an unlikely failure mechanism in well-designed flood defense schemes, nevertheless it remains a possibility during extreme events. If overtopping were to occur the water velocity will increase down the landside slope of the embankment until such time as the water momentum and slope frictional resistance equilibrate and the flow reaches a steady state. This was modelled in this paper as an additional shear stress imparted to the landslide slope surface as per Rossi et al. (Rossi *et al.*, 2021).

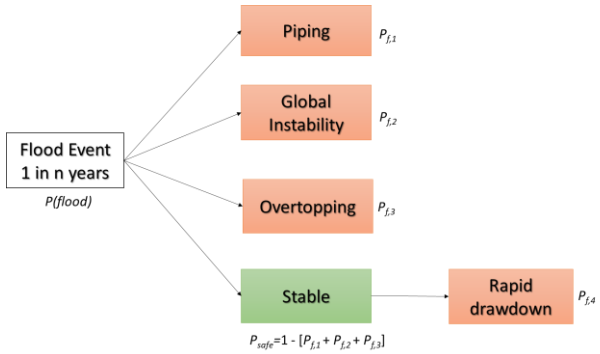

Figure 4 Event tree describing the different failure mechanisms possible and how they relate to one another.

Slope instability is often assessed independently of triggering mechanisms as it is not always clear what event will trigger a landslide (Zhang *et al.*, 2011, Reale *et al.*, 2015,). In this paper, failure mechanisms have been analysed independently as well as systematically using the event tree shown in Figure 4 to combine the individual failure probabilities by considering the chain of events necessary to trigger them (Reale et al., 2016). This framework assumes that the dyke

can fail in one of four ways. Initially after a flood event occurs, the dyke can fail through internal erosion, global instability or overtopping. If the dyke does not fail during this initial phase it may subsequently fail in rapid drawdown, if the water level rapidly retreats following the event. Therefore, the system probability of failure for dyke stability is as described in Eq. 5. For this to occur however, a *1* in *n* year high water event must happen, see Table 1, the actual probability of failure then must consider the flood return period, see Eq. 6.

$$p_{f,sys} = p_{f,1} + p_{f,2} + p_{f,3} + p_{safe}p_{f,4} \quad (5)$$

$$p_{hazard} = p_{flood}p_{f,sys} \quad (6)$$

3.2. Probabilistic analysis

Probabilistic analysis allows the user to explicitly consider design uncertainties, such as inherent material variability or stratigraphical uncertainty, within their design. Accounting for uncertainty within design allows engineers to better understand the system they are designing and gives a true measure of conservatism, unlike factored design approaches. This allows engineers to make more informed decisions and reduce the risk of failure. To perform a probabilistic analysis, uncertain parameters are considered as distributions based on their underlying variability. These distributions are then used in subsequent calculations in place of fixed parameter values. If distributions are used as inputs then the output will be a distribution describing the safety of the system. Such a distribution allows one to consider the probability of the system in question failing and offers a much more meaningful insight into safety than a traditional deterministic factor of safety calculation (determined using unique estimates of the load and resistance). The performance function g(X) or limit state function of an engineered system is expressed as the difference between the system's capacity, C (resistance) and its demand, D (load), see Eq. 7, this is closely linked to a systems factor of safety which is its capacity divided by its demand.

$$g(X) = (C - D)\begin{cases} > 0, \text{safe state} \\ = 0, \text{limit state} \\ < 0, \text{fail state} \end{cases} \quad (7)$$

$$g(X) = g(x_1, x_2, \dots, x_n) \text{for i} = 1 \text{ to n}$$

where X is a vector containing the different random variables (x_i) required to model the slopes safety. Safety is typically expressed either in terms of a reliability index, β, or a probability of failure, p_f. In this paper, we will refer to the probability of failure (p_f) which is defined as the probability of the performance function being less than zero, see Eq. 8.

$$P_f = P[g(X) \leq 0] \quad (8)$$

3.3. Fragility curve generation

Fragility curves describe the conditional probability of reaching or exceeding a certain damage state when a hazard of a known intensity occurs (Martinović *et al.* , 2018; Rossi *et al.*, 2021). They can be used in combination with vulnerability assessments to comprehensively describe the risk profile at the site and provide a rational scalable basis for making risk-based remediation decisions. The fragility curves developed in this study will focus on Dyke failure should a flood of a certain magnitude occur, therefore they will take the following form.

$$p(f|h) = \text{Capacity}(h) - \text{Demand}(h) \quad (9)$$

where h describes the flood height.

4. RESULTS AND DISCUSSION

Fragility curves were developed to assess the likelihood of failure given the occurrence of a flooding event, using the failure states described in section 3.1 and the methodology outlined in sections 3.2 and 3.2.

To develop an internal erosion fragility curve permeability and soil unit weight were considered as probabilistic variables. Typically in-situ permeability has very large, coefficients of variation (COV) (Phoon and Kulhawy, 1999) as the presence

of any cobbles, boulders, air cavities, vegetation, burrows, cracks etc. will significantly alter infiltration, flow path and flow rate. Unfortunately, permeability was not measured at the site and had to be assumed. If permeability is measured the produced internal erosion curve is likely to change.

In this study a mean sand permeability value of 2×10^{-5} m/s was assumed for the sand layer, while four different COVs were considered {0.1, 0.2, 0.3 and 0.4}. Figure 5 shows the results of this analysis, It can be seen that at a COV of 0.4, a 1 in 10 year flood event of 2.75m, would have a probability of instigating an internal erosion failure of 7×10^{-3}, while at a COV of 0.1 the probability is almost two orders of magnitude lower at 6×10^{-5}. In general internal erosion failure does not appear to be significant for flood events lower than the 1 in 1000 year event (3.342m), but beyond this point it quickly becomes the dominant failure mechanism at higher COVs, which one would expect at high permeability.

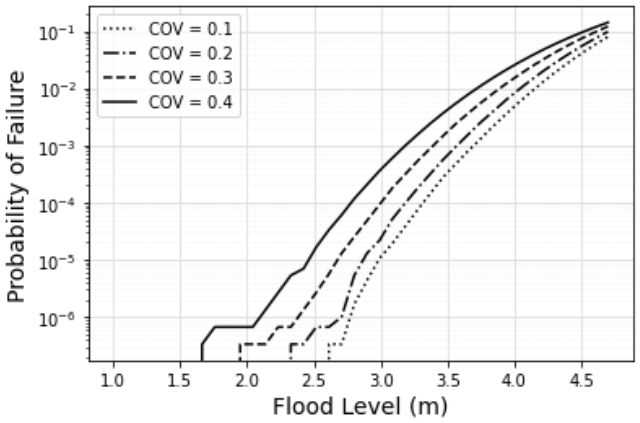

Figure 5 Fragility curve showing the effect of increasing the coefficient of variation of the soil permeability.

A combined fragility curve for global stability and overtopping was generated using the geometry and geotechnical interpretation and parameter variation outlined in section 2. The results are shown in Figure 6. For flood heights in excess of the dyke height of the dyke, additional shear stress caused by overflowing water is included in the analyses. It should be noted that overtopping is extremely unlikely to occur at Oostmolendijk, Table 1 shows that a 1 in 100,000 year flood level wouldn't to overtop the dyke, rendering such calculations unnecessary. The calculation is included herein merely for illustrative purposes. The more likely 1 in 100 year flood event produces a probability of global instability of just below 1%. Which would be considered below average verging on poor when using the USACE (1999) target reliability criteria. The situation isn't markedly improved when considering the 1 in 10 year flood event and as such the safety margin of the embankment during flood events is less than desired. At likely flood heights global instability is the dominant failure mechanism at Oostmolendijk.

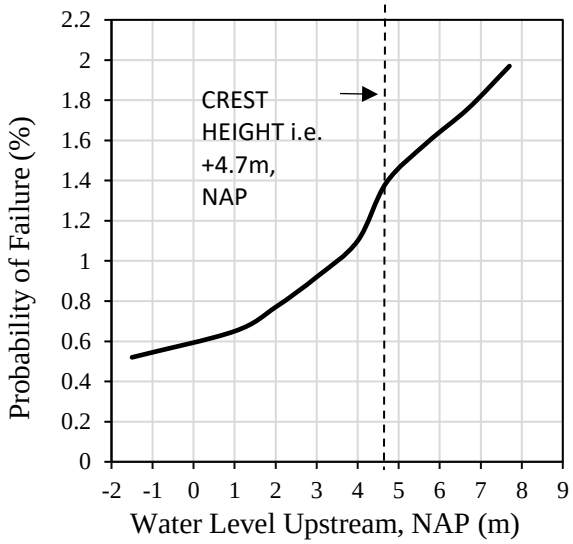

Figure 6 Fragility curve showing the change in global stability as flood level changes

The probability of Oostmolendijk failing during a rapid drawdown event as the river returns to its normal level following a major flood event is the final failure mechanism being considered. The analysis results are depicted in Figure 7, with the curves starting on the left-hand side at the highest water level for a given flood event (for instance, 3.342 m for a 1:1000 year flood). The likelihood of failure then depends on the total change in head height, and the probability of failure increases as the drawdown level increases (i.e., the water level drops on the river side). For 1 in 10, 1 in 100, and 1 in 1000 year drawdown events, the probability of failure ranges from 0.06 to 0.07.

Using the event tree outlined in Figure 4 and Eq. 5, the results from the internal erosion, global stability and rapid drawdown failure mechanisms

were combined to produce a fragility curve which describes the system probability of failure, see Figure 8. The global stability fragility curve dominates this curve until the flood level surpasses 3 m, at which point internal erosion becomes the dominant failure mechanism. A 1 in 100 year flood event has a probability of failure of 1%, which is a cause for concern. Although it should be mentioned that this curve does not take the likelihood of triggering events into account and as a result the actual probability will be lower.

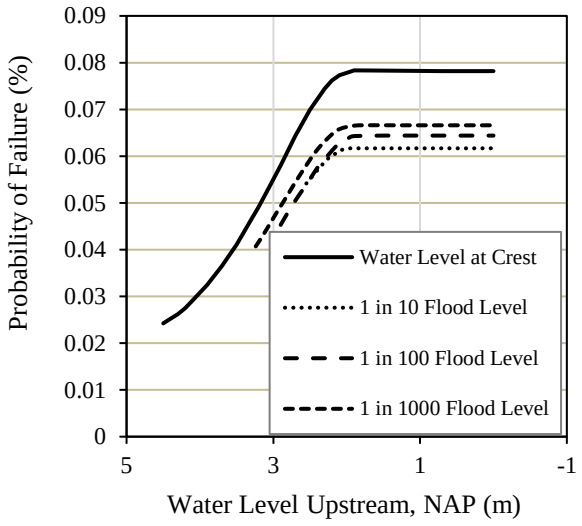

Figure 7 Fragility curve showing the change in stability following rapid drawdown

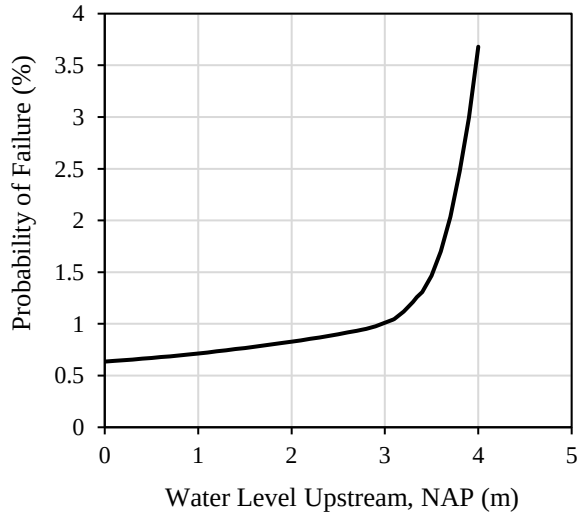

Figure 8 Combined system probability of failure curve

In the absence of a flood event Oostmolendijk has an undesirable probability of failure, driven in large part by the low undrained shear strength in its bearing layers.

5. CONCLUSIONS

A methodology was presented for developing fragility curves to assess the likelihood of dyke failure due to flooding. A number of distinct failure mechanisms were considered individually and systematically, and the dominant failure mechanism was found to be dependent on the flood height. At low flood heights global instability was dominant while internal erosion become more likely as flood height increased. It should be noted that this depends on the soil layering present and should not be generalised. Permeability was not measured at the site and was assumed based on values from the literature, having test data on permeability would reduce uncertainty in the response. A limitation of the methodology is it does not currently consider settlement as a failure mechanism, while in reality excessive settlement will cause progressive spreading of the dyke and will require repair and is quite likely due to the consolidation of the soft clay and peat layers.

Fragility curves such as those generated here can visually allow infrastructure managers to see how their assets are likely to behave as triggering events occur and can be used as the basis for maintenance and remediation decisions. The methodology can easily be adapted for other linear infrastructure networks such as road and rail embankments. They can also be used to justify proactive maintenance and risk scheduling (Stipanovic et al., 2021), giving infrastructure managers a logical framework, they can use to compare assets allowing attention and budget to be allocated to critical assets (Martinović et al., 2016).

It should be noted that Waterschap Hollandse Delta have since carried out additional site and laboratory investigations that have not been processed in this paper and will further understanding when interpreted.

6. REFERENCES

Fugro (2020) Geotechnisch Onderzoek, Grondonderzoek primarie waterkingen 2018-

2022, 17-3. Document nr. 1318-0180-000, Versie 2, Datum 03/02/2020.

Hicks, M. A., Varkey, D., van den Eijnden, A. P., de Gast, T., & Vardon, P. J. (2019). On characteristic values and the reliability-based assessment of dykes. Georisk: assessment and management of risk for engineered systems and geohazards, 13(4), 313-319.

Martinović, K., Gavin, K., & Reale, C. (2016). Development of a landslide susceptibility assessment for a rail network. Engineering Geology, 215, 1-9.

Martinović, K., Reale, C. and Gavin, K. (2018) 'Fragility curves for rainfall-induced shallow landslides on transport networks', Canadian Geotechnical Journal, 55(6), pp. 852–861. doi: 10.1139/cgj-2016-0565.

Morgenstern, N. R. and Price, V. E. (1965) 'The analysis of the stability of general slip surfaces', Geotechnique, 15(1), pp. 79–93. doi: 10.1680/geot.1965.15.1.79.

Phoon, K. and Kulhawy, F. (1999) 'Characterization of geotechnical variability', Canadian Geotechnical Journal, 36(4), pp. 612–624.

Reale, C., Xue, J., Pan, Z., & Gavin, K. (2015). Deterministic and probabilistic multi-modal analysis of slope stability. Computers and Geotechnics, 66, 172-179.

Reale, C., Xue, J., & Gavin, K. (2016). System reliability of slopes using multimodal optimisation. Géotechnique, 66(5), 413-423.

Rijkswaterstaat (2014) The National Flood Risk Analysis for the Netherlands,.

Robertson, P. (1990) 'Soil classification using the cone penetration test', Canadian Geotechnical Journal, 27(1), pp. 151–158.

Rossi, N. et al. (2021) 'Development of Fragility Curves for Piping and Slope Stability of River Levees', Water 2021, Vol. 13, Page 738, 13(5), p. 738. doi: 10.3390/W13050738.

Sellmeijer, J. B. (1988). On the mechanism of piping under impervious structures.

Stipanovic, I., Bukhsh, Z. A., Reale, C., & Gavin, K. (2021). A multiobjective decision-making model for risk-based maintenance scheduling of railway earthworks. Applied Sciences, 11(3), 965.

US Army Corps of Engineers (1999) Risk based analysis in geotechnical engineering for support of planning studies, engineering and design.

Zhang, J., Zhang, L. M., & Tang, W. H. (2011). New methods for system reliability analysis of soil slopes. Canadian Geotechnical Journal, 48(7), 1138-1148.